Study of the Pt (111)|electrolyte interface in the region close to neutral pH solutions by the laser induced temperature jump technique.

P. Sebastián, R. Martínez-Hincapié, V. Climent*, J. M. Feliu*

Instituto de Electroquímica, Universidad de Alicante, Apdo. 99, Alicante, Spain

E-mail: juan.feliu@ua.es

ABSTRACT:

The laser-induced temperature jump method is used to determine the potential of maximum entropy (pme) of a Pt(111) single crystal electrode in contact with an aqueous solution, in a wide pH range and in the absence of specifically adsorbed anions. For this purpose, buffer solutions composed of a mixture of NaF and $HClO_4$ are used. The results are compared with those from non-buffered perchlorate solutions. The use of the NaF/HF buffer allows extending the pH range from 3 to 6, approaching the situation of a neutral pH. Laser experiments show that the pme appears located at nearly the same potential position in the whole pH range between 3 and 6. This value is around 300 mV vs SHE, in agreement with previous works. Moreover, the potential response to the fast thermal perturbation at high potentials, above the pme, indicates the presence of a slower contribution, resulting in a bipolar, non-monotonous, profile. Such behaviour is strongly affected by the presence of fluoride anion and/or hydrofluoric acid, thus evidencing a strong structural effect on interfacial water from these species. These results bring some light to the understanding of the interfacial properties in acid-neutral conditions, and also show the influence of different non-specifically adsorbed anions on the interfacial properties that cannot be evidenced only by cyclic voltammetry.

*Corresponding authors:
Victor Climent: victor.climent@ua.es
Juan Feliu: juan.feliu@ua.es

1. Introduction:

The study of the properties of metal aqueous solution interfaces is needed for a better understanding of many electrochemical processes. Water is undoubtedly the most studied solvent in electrochemistry and plays a capital role in interfacial studies. Both the way in which water molecules are structured in the interfacial region and the nature of the interaction between them and with the metal surface electrode will have a great influence in the electrocatalysis and reactivity of electrochemical systems [1-4]. Particularly interesting is the study of the effect of the pH on the properties of the interphase [5-8]. In this regards, solutions with pH close to neutrality are of special relevance in a wide range of fields such as bioelectrochemistry and biotechnology, in which interfacial phenomena are widely present.

To perform these fundamental studies, platinum electrodes with well-defined surfaces are of particular interest, since this metal is one of the most active catalysts for many important reactions, in addition of being considered as model electrode material. However, the platinum electrode|electrolyte interphase cannot be considered as ideally polarizable in a sufficiently wide range of potentials [9, 10]. Reversible adsorption/desorption processes involving electron transfer take place on Pt electrodes and they complicate the study of interfacial properties. As a consequence, the determination of the potential of zero charge (*pzc*), a key parameter in the description of electrified interphases, becomes quite challenging. In this regards, it has been previously emphasised the necessity of distinguishing between total charge (including charge involved in adsorption processes) from free charge, the purely interfacial charge. While the latter is the one that controls in great extend the electric field at the interphase, its determination is not always possible [9]. The use of CO charge displacement technique allows the determination of the total charge and the potential of zero total charge (*pztc*) of platinum electrodes [11, 12]. From this knowledge of the total charge it is also possible to estimate the potential of zero free charge (*pzfc)*, but only in the case of Pt(111). In this case, it is possible to take advantage of the fact that, on this electrode, in the absence of specific anion adsorption, hydrogen and hydroxyl adsorption regions are separated by what is generally accepted as

a double layer region. In this region, total and free charges almost coincide within experimental error. By extrapolation of the interfacial voltammetric charge in the double layer region and taking into account some considerations, the location of the *pzfc* can be estimated [11, 13, 14]. Previous works made in perchlorate acid solutions within the pH range between 1 and 3, showed that *pzfc* of the interface Pt(111) | perchlorate solution appears located at almost the same potential position in the SHE scale, while most voltammetric features shift 59mV per pH unit to more negative potentials [15]. In a more recent work, the use of the buffer formed by *x* M $HClO_4$ and 0.1 M NaF mixtures allowed to extend the pH range until pH 5, without any influence of specific anion adsorption [16]. The results obtained with those mixtures agree with those obtained in more acidic media providing values of *pzfc* close to 320-330mV vs SHE in all cases. This result suggests again the non-pH dependence of the extrapolated *pzfc*. The *pzfc* of rough platinum electrodes was determined in the past by alternative methods [17, 18]. One of them is the direct measurement of the change of pH when a high surface area electrode is brought into contact with the solution. A nearly independent *pzfc* value was also determined in this case for Na_2SO_4 solutions with pH ranging from 3 to 6. Values of *pzfc* of rough platinum electrodes in different electrolyte solutions are summarised in [17]

An alternative approach to estimate the *pzfc* of Metal | solution interfaces is the use of the laser induced temperature jump technique [19, 20]. By using short laser pulses (5ns), the temperature of the interface can be suddenly raised, resulting in a displacement of the potential of the electrode under coulostatic conditions [21, 22]. The potential difference at the interphase has contributions from the work function of the metal, including the spillover of the electrons, and the dipolar contribution of the network of solvent molecules. The latter is the most influenced by the thermal perturbation while the effect of the temperature on the other contributions is, in comparison, nearly negligible [23, 24]. Hence, the response of the interface to the sudden temperature change is mainly dominated by the reorganization of the network of water molecules close to the surface after the laser pulse. The sudden increase of the temperature disorders the water network decreasing its dipolar contribution to the overall potential drop [25]. The sign of this dipolar contribution is mainly determined by the free charge on the

metal. At potentials lower than the *pzfc* the net orientation of water molecules is with the hydrogens towards the surface and the solvent dipolar contribution is positive. In this case, the response obtained from the laser temperature jump is a negative potential transient. On the other hand, at potentials higher than the *pzfc*, the surface is positively charged and water dipoles contribute negatively to the electrode potential, being mainly oriented with the oxygen towards the surface [25-27]. Then, the potential transient obtained in this case is positive. Therefore, valuable information about the orientation of water dipoles at the interphase is provided by this relaxation technique. The potential at which the laser induced transient approaches zero coincides with an initial situation of minimum net dipolar contribution equivalent to a maximum disorder of the network of water molecules. This potential value is the potential of maximum entropy (*pme*) which, according to the previous discussion, is closely related to the *pzfc*. The measured potential transient contains also dynamic information, and due to the short time scale of this experiment, different processes with different rates can be decoupled. Usually, the double layer reorganization is almost instantaneous, while other processes like hydrogen and anion adsorption/desorption respond with lower rates, providing extra information about the metal-solution interface[21].

In the present work the interface Pt(111) | aqueous solution is studied for the first time by the laser temperature jump technique in a wide pH range between 3 and 6. For that, different mixtures of (0.1-*x*) M NaF + *x* M($HClO_4$) were used to prepare the solutions at different pHs. These particular mixtures were selected because neither fluoride nor perchlorate anions adsorbs specifically on Pt(111). Results obtained are compared with those gained using unbuffered perchlorate solutions.

2. Experimental:

Before each experiment, the Pt(111) electrode was flame annealed and cooled down to room temperature in a reductive atmosphere[28]. For that, a flow of H_2 and Ar in the ratio 1:3 was passed through pure water in a round bottom flask for several minutes. The Pt(111) electrode was cooled down in this atmosphere for several seconds, contacted with the water in equilibrium with the H_2/Ar gas

mixture and transferred to the working cell protected with a drop of this water. A Pd wire, charged with H_2, was used as a reference electrode whereas a Pt wire was used as a counter electrode. A second Pt wire was required and used as a second working electrode in order to carry out the laser temperature-jump measurement [22]. The experiments were performed with the Pt(111) electrode in the hanging meniscus configuration.

Cyclic voltammograms were recorded using a μ-Autolab III potentiostat (Eco-Chemie, Utrecht, The Netherlands) under the current integration mode.

The pH values of the different solutions were measured using a *PH-basic-20* pH-meter from Crison coupled with a pH-probe pH 50 12 HACH model. Cross-checking of pH values using hydrogen evolution reaction was also employed.

The procedure for recording the laser transients was described in detail elsewhere [21, 22]. Before recording the laser transient, several voltammetric cycles were recorded to ensure the cleanliness and stability of the system. Afterwards, a second auxiliary electrode was connected to be used as an internal reference to measure the potential transient. At the beginning, both working and the second auxiliary electrode are polarized at the same potential. Approximately 200 μs before firing the laser both electrodes are disconnected from the potentiostat. In the absence of faradaic reaction, the potential of the electrode should remain at the value previously imposed. Small traces of O2 cause a slow drift of the open circuit potential towards the oxide region. However, this drift is negligible in the microsecond time scale. Due to the laser irradiation, the temperature at the interphase rises 25-50 degrees with in the duration of the pulse, 5 ns. However, the temperature drops very fast and after 1 μs the remaining temperature change is only ca. 1-2 degrees. The potential difference between both electrodes is measured at open circuit. As the laser pulse only affects the single crystal working electrode, the measured potential difference is related to the response of such interface. Each experiment is repeated with a frequency of 10Hz to ensure that the temperature relaxes to the initial value between measurements. The potentiostat is reconnected between successive laser pulses to keep the potential at the desired value. In that way 128 or 256 potential transients are recorded and averaged using a Tektronix Model TDS 3054B oscilloscope. Finally, after recording all potential transients the cyclic

voltammetry was registered again to check the stability of the system and cleanliness of the interphase.

The duration of the pulse is 5ns and the laser used is a 532 nm frequency (double harmonic) Nd-YAG (Brilliant B from Quantel). A special arrangement of lenses is used both to reduce the initial diameter of the laser beam from 6 mm to 4 mm and also to direct the laser beam to the cell which is kept in a Faraday box to avoid electrical noise during the measurement. The energy density of the laser beam is reduced to 10-16 mJ/cm^2. The reduction of the energy beam is achieved by combining the effect of an attenuator from Newport Corporation (Model M-935-10) and the regulation of the Q-switch time. The laser energy was measured with a pyroelectric sensor head (Model M-935-10).

3. Theoretical considerations:

As the energy density of the applied laser beam is low enough to avoid the damage or the photoemission of electrons from the platinum surface (the work function of Pt(111) is ca. 5.9-6.10 e.V [29-32]) it is considered that the only effect caused by the laser illumination is a sudden increase of the temperature of the interface. The change in the temperature cannot be directly measured due to the short time scale of the phenomenon, but it can be estimated by applying a simple thermal transfer model, just considering that the non-reflected portion of energy is immediately converted into heat[22]:

$$\Delta T = \frac{2I\,(1-R)}{\sqrt{\pi}}\left[\frac{k}{\sqrt{\boldsymbol{\alpha}}}+\frac{k_1}{\sqrt{\alpha_1}}\right]^{-1}\left(\sqrt{t}-\sqrt{t-t_0}\right)(t>t_0) \qquad (1)$$

Where I (Wcm^{-2}) is the laser intensity, considered spatially uniform, R is the reflectivity of the surface, t_0 is the duration of the laser pulse, 5ns, and κ (Wcm^{-1}K^{-1}), α (cm^{2}s^{-1}) and κ_1, α_1 are the thermal conductivity and the thermal diffusivity of the metal and the aqueous solution, respectively.

For long decaying times ($t>>t_0$) the above expression can be simplified to:

$$\Delta T = \frac{1}{2}\boldsymbol{\Delta} T_0\sqrt{\frac{t_0}{t}} \qquad (2)$$

Where ΔT_0 is the maximum temperature change. The response of the (open circuit) potential to the thermal perturbation, under coulostatic conditions, follows

the change in the temperature. If the reorganization of the interface is faster than the time scale of the temperature perturbation and the change of the temperature is sufficiently small (this is at $t>>t_0$), the change of the potential will be given by:

$$\Delta E = \frac{1}{2}\left(\frac{\partial E}{\partial T}\right)_q \Delta T_0 \sqrt{\frac{t_0}{t}} \quad (3)$$

Where the term $\left(\frac{\partial E}{\partial T}\right)_q$ is the thermal coefficient of the double layer that can be extracted from the slopes of ΔE vs $1/\sqrt{t}$ (provided ΔT_0 is known).

In addition to the change of potential due to the double layer reorganization, another contribution should be added to the equation above, i.e, the potential drop caused by the temperature difference that exists between the reference electrode and the working electrode. This is called the thermodiffusion potential and can be estimated from the Eastman entropies of transport of the different ions from the electrolyte[33]:

$$\frac{\Delta E_{thermodiffusion}}{\Delta T} = -\frac{1}{F}\sum \frac{t_i}{z_i} S_i \quad (4)$$

where t_i, z_i and S_i are the transport number, the charge and the Eastman entropy of transport of the ion *i*, respectively.

As it will be shown later, the potential change due to thermodiffusion phenomena is very small and can be neglected in most cases. Thus, we can consider that the major contribution to the potential transient comes from the double layer response after the laser pulse.

In those cases where an electrosorption process (hydrogen or anion adsorption) can take place, this will be coupled with the change of the potential induced by the reordering of water dipoles and normally opposes to it, resulting in a deviation from the monotonous decay predicted by equation (3). The rate and direction of the adsorption/desorption process will be dominated by the overvoltage:

$$\eta = E - E_{eq} = \Delta E - \Delta E_{eq} \quad (5)$$

Where ΔE and ΔE_{eq} represent the difference of the electrode potential and the equilibrium potential of the adsorption process, respectively, with the initial potential, E_i. At the beginning, before the temperature perturbation, ΔE_{eq}=0, because the system is initially at equilibrium. When the temperature is changed, E_{eq} changes, mainly because the equilibrium depends on the temperature. On

the other hand, equation (3), representing the change of the potential, should now be modified to include also the effect of adsorption:

$$\Delta E = \left(\frac{\partial E}{\partial T}\right)_{q,\theta} \Delta T + \nu_i \frac{q_{ML}}{C_{dl}} \Delta\theta \qquad (6)$$

where q_{ML} is the charge transferred upon the adsorption of a monolayer, C_{dl} is the double layer capacity, θ is the coverage (of atomic hydrogen or hydroxyl species, in the present case) and ν_i is +1 for the reductive adsorption of a cation (H^+) and -1 for the oxidative adsorption of an anion (OH^-). For a positive value of the thermal coefficient of the double layer, $\left(\frac{\partial E}{\partial T}\right)_{q,\theta}$ the change of potential after the temperature increase will be initially positive. If $\Delta E > \Delta E_{eq}$ (this will depend mainly on the relative values of $\left(\frac{\partial E}{\partial T}\right)_{q,\theta}$ and $\left(\frac{\partial E_{eq}}{\partial T}\right)_{\theta}$) coverage will decrease for cation and increase for anion adsorption. In both cases the term $\nu_i \frac{q_{ML}}{C_{dl}} \Delta\theta$ is lower than zero, therefore opposing to the initial change due to the dipolar term. A similar conclusion is obtained for $\left(\frac{\partial E}{\partial T}\right)_{q,\theta} < 0$. In this case, $\nu_i \frac{q_{ML}}{C_{dl}} \Delta\theta > 0$, again opposing to the dipolar contribution. The exact shape of the potential transient can be calculated after introducing an equation to account for the kinetics of the reaction:

$$\frac{d\theta}{dt} = f(T, \theta, \eta) \qquad (7)$$

The Butler-Volmer relationship has been previously used for the calculation of the laser induced potential transients. For a small temperature perturbation, the function *f* can be linearized and equation (7) can be written as:

$$\frac{d\theta}{dt} = -\nu_i \frac{j}{q_{ML}} = -\nu_i \frac{\eta}{R_{ct} q_{ML}} \qquad (8)$$

Where R_{ct} is the charge transfer resistance for the adsorption/desorption process. Under this condition the following equation results:

$$\Delta E = \left(\frac{\partial E}{\partial T}\right)_{q,\theta} \Delta T + \frac{\xi}{\tau} \int_0^t \exp\frac{t-x}{\tau} \Delta T(x) dx \qquad (9)$$

Where the first term represents the fast response of the double layer and the second term the slow response of an adsorption/desorption process with time constant τ. The proportionality constant for the slow response ξ is given by:

$$\xi = -\frac{q_{ML}}{C_{dl}} \frac{\left(\frac{\partial E}{\partial T}\right)_{q,\theta} - \left(\frac{\partial E_{eq}}{\partial T}\right)_{\theta}}{\frac{q_{ML}}{C_{dl}} - \nu_i \left(\frac{\partial E_{eq}}{\partial \theta}\right)_T} \quad (10)$$

And the time constant is related with the charge transfer resistance by:

$$\tau^{-1} = \frac{1}{q_{ML} R_{ct}} \left(\frac{q_{ML}}{C_{dl}} - \nu_i \left(\frac{\partial E_{eq}}{\partial \theta}\right)_T \right) \quad (11)$$

For intermediate coverages the term $\left(\frac{\partial E_{eq}}{\partial \theta}\right)_T$ is small and $\tau \cong R_{ct} C_{dl}$

For $t \gg \tau$ equation (9) reduces to:

$$\Delta E = \left(\frac{\partial E}{\partial T}\right)_{q,\theta} \Delta T + \xi \Delta T \cong \left(\frac{\partial E_{eq}}{\partial T}\right)_{\theta} \Delta T \quad (12)$$

In summary, the open circuit potential changes with temperature according to the equilibrium potential. On the other hand, when the rate constant of the adsorption/desorption process is too small to follow the fast thermal perturbation, $t \ll \tau$, an effective decoupling of such processes from the double layer response is achieved.

4. Results and discussion:

Figure 1 shows the cyclic voltammetries recorded in (0.1 - *x*) M NaF + *x* M $HClO_4$ mixtures of different pH. The voltammograms are very similar to those recorded in 0.1 M $HClO_4$ and in (0.1-*x*) M $KClO_4$ + *x* M $HClO_4$ mixtures. Therefore, no evidence of fluoride specific anion adsorption is observed, as expected from previous literature [16, 34-38]. At low potentials (*E*<0.4V), hydrogen adsorption takes place whereas at higher potentials (*E*>0.5 V) the voltammogram is dominated by hydroxide adsorption. By increasing the pH, the characteristic sharp spike around 0.80 V vs RHE decreases progressively in both sharpness and intensity while the charge related to the overall hydroxide adsorption region increases slightly. These features evidence a strong reorganization of the charge located in the interfacial region caused by the pH change. In fact, the cyclic voltammogram evolves with increasing pH, approaching the profile recorded in alkaline media, where no sharp spike is present [39, 40]. In the potential region where hydrogen adsorption takes places, the charge remains almost invariable [16] with a value around 150 μCcm^{-2}, slightly lower than the characteristic value

in 0.1 M $HClO_4$, 160 μCcm^{-2} . At pH 6 the cyclic voltammogram becomes slightly irreversible, especially in the most positive potential region, evidencing that this pH value is the upper limit for the buffering capacity of HF/F^- mixtures (Figure 1B,d). It is noteworthy that the current in the double layer region becomes remarkably low for the higher pHs investigated. The following can be an explanation for the decrease of double layer current: the small broad peak observed in pH 3 around 500mV vs RHE (i.e., in the double layer region), does not shift with pH, while hydrogen and hydroxyl adsorption currents shift nearly 59 mV/pH unit as predicted by Nernst law. At pH 6 the broad peak, previously in the double layer region, is completely coupled within the hydroxyl region and therefore is not visible anymore. The displacement of this feature outside the double layer region is most likely the reason for the significant decrease of the double layer current.

Figure 2 contains the laser transients obtained for Pt(111) in contact with (0.1- x) M NaF + x M $HClO_4$ aqueous solutions, at four pH values. At low enough applied potentials, the transients measured are, in all the cases, negative, $\left(\frac{\partial E}{\partial T}\right)_{q,\theta} < 0$, and monotonically relax to zero with time. The transients recorded within the potential region where hydrogen adsorption/desorption takes place show only the negative and fast response expected from the disordering of the double layer. Only at pH 3, the potential transient at low potential values (Figure 2A,a, in red) shows a small contribution from the hydrogen adsorption/desorption process, evidenced as a deviation from the monotonous decay predicted by equation (3). This slow contribution is completely suppressed at higher pHs [21], i.e by decreasing the bulk protons concentration. When the applied potential is increased, the magnitude of the transient decreases and its sign eventually turns positive, $\left(\frac{\partial E}{\partial T}\right)_{q,\theta} > 0$, pointing out that the change in the orientation of the water molecules has taken place. At the particular potential where the transient approaches to zero, $\left(\frac{\partial E}{\partial T}\right)_{q,\theta} = 0$, the net orientation of the water molecules is negligible, indicating the location of the *pme*.

Figure 3 shows the laser transients recorded at more positive potentials, in the potential region dominated by hydroxide adsorption [40, 41]. At those potentials,

the transients are non-monotonous, with an initial positive fast response followed by a negative, slower contribution, which finally relaxes to zero. As the potential of the experiment is increased, the negative contribution becomes more prominent, turning completely negative at the highest potential range, where the surface is covered by oxide [42]. This bipolar behaviour evidences that at least two processes with different time constants are sensitive to the temperature perturbation, overlapping in the overall laser response. It must be highlighted that the bipolar behaviour observed in NaF+$HClO_4$ mixtures is not observed in non-buffered perchlorate solutions of pH>3, as it was previously reported [26].

The experiment shown in figure 4 illustrates this point. Figure 4A compares the cyclic voltammetries of Pt(111) in contact with a solution resulting from a mixture of (0.1-*x*)M NaF+ xM $HClO_4$ (x=0.03, pH 3.2), and a solution composed by 0.1M $KClO_4$ +0.001M $HClO_4$, of similar pH. As it can be seen, both cyclic voltammetries are essentially the same, just evidencing that neither fluoride nor perchlorate adsorb specifically on Pt(111). However, the laser transients recorded in the high potential region for the 0.1M $KClO_4$ + 0.001M $HClO_4$ solution differ from those recorded in the NaF +$HClO_4$ solution of the same pH. In the low potential region, e.g. below the *pme*, the transients are essentially identical (Figure 4B). However, at more positive potentials, above the *pme*, the transients recorded in the absence of fluoride are higher in magnitude and show only a positive response with a monotonous decay following the temperature relaxation after the laser pulse. Only at the most positive potential, 1.0 V RHE, i.e, well above the hydroxyl adsorption region [40, 41], the transient changes its sign. It should be pointed out that some slow negative contribution was previously observed in this potential region at pH=1 (0.1 M $HClO_4$) and attributed to the participation of the OH adsorption/desorption reaction on the transient response [26]. The rate of this reaction would decrease with the increase of the pH and would be almost negligible at pH=4. On the other hand, the laser induced potential transients recorded in the solution that contains fluoride anions (Figure 3) show a non-monotonous decay, as discussed previously, that start with a fast positive response, followed by a slower negative contribution. The influence of the presence of fluoride on the shape of the transients varies with pH. At pH around 5, (Figure 3C) the magnitude of the slower component of the response start to

decrease and becomes almost negligible at pH close to 6 (Figure 3D). This is the same trend observed in (0.1-x) M $KClO_4$ + x M $HClO_4$ solutions but in a shifted pH range.

The observation of a slow response even at pH=5 in solutions containing mixtures of NaF and $HClO_4$, could be interpreted as a catalytic effect on the rate of OH adsorption due to the presence of fluoride even although this anion does not adsorb on the surface. Incidentally, in previous work [43] it was shown that the presence of some anions at very low concentration exert important changes in the voltammetric profile in the hydroxyl adsorption region. Such effect was rationalized considering the capacity of some anions to induce water ordering whereas other anions cause disordering in the structure of water [44, 45]. Thus, the type of anion present in the electrolyte could have a great influence in the interfacial properties of Metal|Solution interfaces even in the absence of adsorption [46]. In particular, fluoride is an anion expected to favour the formation of structured water [35, 43].

In order to investigate in more detail the possible role of the pair HF/F on the structure of the double layer, different solutions at pH 4 were prepared varying the concentration of the buffer NaF+$HClO_4$, and adjusting the ionic strength to 0.1M with $KClO_4$ (a possible cation effect is neglected in the potential region of interest, i.e potentials positive to the *pztc* and absence of specific anion adsorption). Although the buffer capacity changes, the small amount of protons involved in the adsorption processes will presumably not modify the interfacial pH value. The pH was fixed to 4 (by adding the proper amount of $HClO_4$) since this pH showed the greatest influence from HF/F^- to the laser response (see Figure 3B). Figure 5 contains the cyclic voltammetry for three different buffer concentration solutions: (0.1-*x*) M $KClO_4$ + *x* M NaF/$HClO_4$ buffer where *x*= 0.05 , 0.02 , 0.01 respectively. As expected, the cyclic voltammograms overlap quite well in the overall potential window under scope not showing any voltammetric feature related with the losing of buffering capacity. Interestingly, the response to the laser heating differs for each buffer solution, showing a clear trend with the decrease of total HF/F^- concentration. Figure 6 (A,B and C) contains the laser transients at three potential values recorded in the hydroxyl potential region: 700mV, 800mV and 900mV vs RHE, for the three buffer concentrations

employed. Comparison of these potential transient clearly shows that the negative response becomes slower as the total concentration of HF + F^- decreases. At 0.05M NaF/$HClO_4$ buffer (Figure 6A) the ΔE *vs t* transient still shows contributions from the fluoride presence, but those become almost negligible, employing the same time scale, for the 0.01M NaF/$HClO_4$ buffer concentration (Figure 6C). At this concentration, the laser transients have increased in magnitude and show only the fastest double layer reorganization response. Hence, the bipolar response seems to follow the kinetics of a process that could be regulated by the presence of HF/F^- species. Finally, figure 6D contains the whole group of laser transients for the solution 0.09M $KClO_4$ plus 0.01M NaF/$HClO_4$ buffer, including low potentials. The bipolar response at potentials above the *pme* was completely decoupled thus enabling the straightforward analysis of such transients.

At this stage it is still unclear the nature of the negative slow response induced by the presence of the pair HF/F^-. In the following, we attempt to analyse the transients under the light of the model described previously (equations (5) to (12)). Although this model does not describe quantitatively all the features of the potential transients it can be used to qualitatively justify some of the trends. In this framework, the slower and more negative response at potentials above the *pme*, can be tentatively assigned to the effect of hydroxyl adsorption on the potential transient limited by the kinetics of the reaction, as it was proposed for $HClO_4$+$KClO_4$ mixtures[26]:

$$2H_2O + Pt \leftrightharpoons Pt\text{-}OH + H_3O^+ + e(Pt)$$

Accordingly, the bipolar transient can be understood in the following way: since the potential of the experiment is higher than the *pme*, the dipolar contribution is negative and the initial part of the laser transient will be positive. At very short times, the increase of the electrode potential due to the temperature perturbation shifts the OH adsorption/desorption equilibrium forcing an increase of its coverage. Such adsorption releases electrons to the surface causing a decrease in the electrode potential, therefore opposing to the contribution from the disordering of the solvent dipolar layer. This equilibrium would be too slow to be observed in the time scale displayed in non-buffered perchlorate containing solution, above pH 3. In NaF+$HClO_4$ solutions, however, the electrolyte seems to

affect this process, increasing its rate. This could be due to the kosmotropic (structure making) effect of F^- . The changes in the relative magnitude of the two peaks that conform the butterfly shape of the hydroxyl region in the voltammogram could be reflecting the effect of fluoride on the ratio between free and structured interfacial water.

To simulate the potential transients with equations (5) to (12) some parameters are necessary that can be obtained from the application of a Frumkin isotherm. Figure 7 compares the cyclic voltammogram recorded in pH=4 in the region of hydroxyl adsorption with the simulation of an adsorption process controlled by a Frumkin isotherm using the parameters indicated in table 1. While this oversimplified isotherm is not able to describe all the features observed in the voltammogram, it gives an overall picture of the process sufficient enough to describe the main trends observed in the laser induced transients. Additional information to apply equations (5) to (12) is the variation of some of these parameters with the temperature. Unfortunately, such information is not available for the range of pHs studied in this work, and it is only available for pH 1 [47]. On the other hand, the number of parameters for the simulation is too large to allow obtaining these by fitting experimental data. For that reason, the strategy followed has been the following: starting with the parameters (ΔS^0 and $d\omega/dT$) reported for pH=1, these have been slightly adjusted until good similarity with the laser potential transient measured at 0.75 V in pH=4 is attained. Then, with these parameters fixed, the pH in the simulation has been varied to see the effect predicted by this model on the potential transients (at constant potential). The results are shown in figure 8, where experimental and simulated transients are compared. Observation of figure 8B reveals that the model allows qualitative explanation of some trends, but not all of them. First, as previously discussed, equation (12), the sign of the transient at long times is representative of the contribution $\left(\frac{\partial E_{eq}}{\partial T}\right)_\theta$ which is related with the values of ΔS^0 and $d\omega/dT$. In this respect, the fact that the trend observed at long times can be reproduced by using values of the parameters close to the experimental values measured at pH=1 gives validity to the model. The model also reproduces the increase of the time constant as the pH increases, resulting in the decrease of the magnitude of the negative contribution. However, this decrease is more intense in the experimental

results than on the simulation. This discrepancy can be due to the fact that the model does not consider the limited diffusion of species from the bulk to the surface or the effect of acid / base equilibrium in the species of the buffer near the surface, which will be also affected by the distance to the electrode [48, 49].

The most important discrepancy between the experimental and simulated transients is observed at the more acidic pH. While the model predicts a continuous decrease of the time constant of the slow response (i.e., an increase of the magnitude of the negative contribution), the experiment shows that the time constant decreases (the negative part becomes faster) from pH 5.7 to 4.2 but increases (becomes slower) again at pH=3.2. This trend can be related with the acid-base equilibrium between HF and F^-. As the pH approaches the pK_a of HF, the concentration of F^- decreases and the concentration of HF increases. It is possible that the catalytic species for the reaction is the deprotonated form, F^- and decreasing its concentration increases the time constant of the process.

There is one aspect of the experimental results that cannot be explained with the previous model. At very positive potentials the transients turn completely negative. The model postulated above explains the negative contribution as the result of the increase of OH coverage associated to the change of the potential induced by the laser. However, at potentials above the so-called butterfly feature, the OH adlayer is completed and no change of the coverage is induced by the change of the potential. To illustrate this point, figure 9 shows calculated potential transients using the same parameters used to calculate the transients in figure 8, but varying the electrode potential. It is clear that, as the potential increases, the negative contribution to the potential transient decreases, in contradiction with the experimental result, but in accordance with the intuitive explanation above. Therefore, an additional reason is required to explain the negative transient at very high potentials. This could be related with the superequivalent adsorption of anions (OH) that would screen the electrode charge in such a way that water dipoles are affected by an effective negative charge even although the charge on the metal is positive. Similar trend was also observed for the adsorption of sulfate anions on Pt(111) and Au(111)[21, 22].

Once the nature of negative contribution has been tentatively explained we turn again our attention towards the determination of the *pme*. This parameter can be

obtained more clearly in the solutions with lower HF/F^- concentration to avoid the interference of the slow response, as discussed above. Under these conditions, there is an effective decoupling of the double layer response from the adsorption processes. From the laser transients recorded at different applied potentials, the temperature coefficient of the double layer can be calculated by plotting the ΔE vs $\sqrt{t}$ (Figure 10). From the slopes of the plots ΔE vs $\sqrt{t}$ the values of the coefficient $\left(\frac{\partial E}{\partial T}\right)_{q,\theta}$ are calculated following equation (3). Plotting the values of this coefficient as a function of the potential allows an easy determination of the *pme*. Strictly speaking, the temperature coefficient estimated as indicated above needs a correction from thermodiffusion that, as it was explained in the preliminary section, it is estimated through the Eastman entropies of transports of the ions resulting from the electrolyte. Table 2 contains the Eastman entropies for each ion whereas table 3 contains the $\Delta E_{Thermodiffusion}/\Delta T$ in every case. Those values are very small, almost negligible, so the main contribution to the change of the potential comes from the double layer reorganization. Figure 11 represents the plots of $\left(\frac{\partial E}{\partial T}\right)_{q,\theta}$ vs the applied potential in the SHE scale at pH values ranging from 3 to 6, with and without the thermodiffusion correction: it can be seen that both values nearly overlap. In all the cases the coefficient approaches to cero around 300 mV vs SHE, just indicating that the *pme* would remain constant in the whole pH scale from 3 to 6. That agrees with previous estimations of the *pzfc* from CO displacement technique[16].

To finish this discussion, the *pme* values from (0.1-x)M NaF + xM $HClO_4$ buffer solutions calculated as indicated above were plotted vs the measured pH (Figure 12). This plot also contains the *pme* calculated from the solutions 0.09M $KClO_4$ + 0.01M NaF/$HClO_4$ buffer (open symbols). The dashed line represents a slope of 59mV/decade. From this figure it can be clearly seen that the *pme* moves around 59 mV per pH unit, in the RHE scale, while it is constant in the SHE scale. The linear trend in the RHE scale fits quite well the experimental data for pH > 5. However, for lower pHs, there is a small deviation. This deviation could be related to the difficulty associated to the interference of the slow response associated to the presence of HF/F, as described above. This interference could falsely shift the *pme* slightly, even when the concentration of the buffer is decreased, showing

in this case a little improvement. In conclusion, apart from this small uncertainty, the *pme* values approach approximately to 300mV vs SHE and remains almost constant in the whole acidic pH range up to pH 6. Conversely, the *pme* of other platinum surfaces, lies in the hydrogen adsorption/desorption region and change with pH, suggesting that the *pzfc* also changes with pH in this case[26]. A thermodynamic analysis [17] relates the variation of *pzfc* with pH when this one falls within the hydrogen region, according to the following expression:

$$\left(\frac{\partial E}{\partial \mu_{H^+}}\right)_{\sigma=0,\mu_{salt}} = \frac{1}{F}\frac{1}{1-\frac{1}{F}\left(\frac{\partial \sigma}{\partial \Gamma_H}\right)_{E_r,\mu_{salt}}} \quad (13)$$

According to this expression, if hydrogen adsorption does not involve change in the free charge, $\left(\frac{\partial \sigma}{\partial \Gamma_{\mathrm{H}}}\right) = 0$ and the shift with the pH will be 59 mV/decade. However, when the *pzfc* lies in the double layer region , $\left(\frac{\partial \sigma}{\partial \Gamma}\right) = \infty$ and the *pzfc* is independent of pH.

5. CONCLUSIONS:

The interface Pt(111) in contact with aqueous solution was investigated in a wide pH range. The usefulness of the buffer $HClO_4$/NaF to study the interface Pt(111) | aqueous solution by using the laser induced temperature jump method was demonstrated. Such mixtures offer sufficient buffer capacity without interference of specific anion adsorption, allowing extending the pH range of these studies from pH 3 to pH 6, closer to bulk neutrality. The *pme* estimated was located near to 300mV vs SHE in agreement with previous work made by García-Araez et. al.[26]Those results suggest that the *pzfc* remains constant in the SHE scale being non-pH dependent, while the adsorption features that dominate the cyclic voltammetry shifts 59V per pH unit.

A strong structural effect from the species of the electrolyte was observed, evidenced through the bipolar behaviour that the laser induced potential transients displays at more positive potentials. This particular behaviour was mainly assigned to the effect of fluoride, and its conjugated acid HF, on the

structure of water at the interphase. Such effect would result in a catalysis of the OH adsorption process. Therefore, this system is an example of how the nature of the species of the electrolyte influences the interfacial properties and can affect the rate of the processes that take place in it. More work is needed in order to better understand this phenomenon.

ACKNOWLEDGMENTS:

Support from MINECO (Spain) through project CTQ2016-76221-P and Generalitat Valenciana through project PROMETEOII/2014/013 is greatly acknowledged. RMH thankfully acknowledges support from Generalitat Valenciana under the Santiago Grisolia Program (GRISOLIA/2013/008). PS thankfully acknowledges to the MEC (Spain) for the award of a FPU grant.

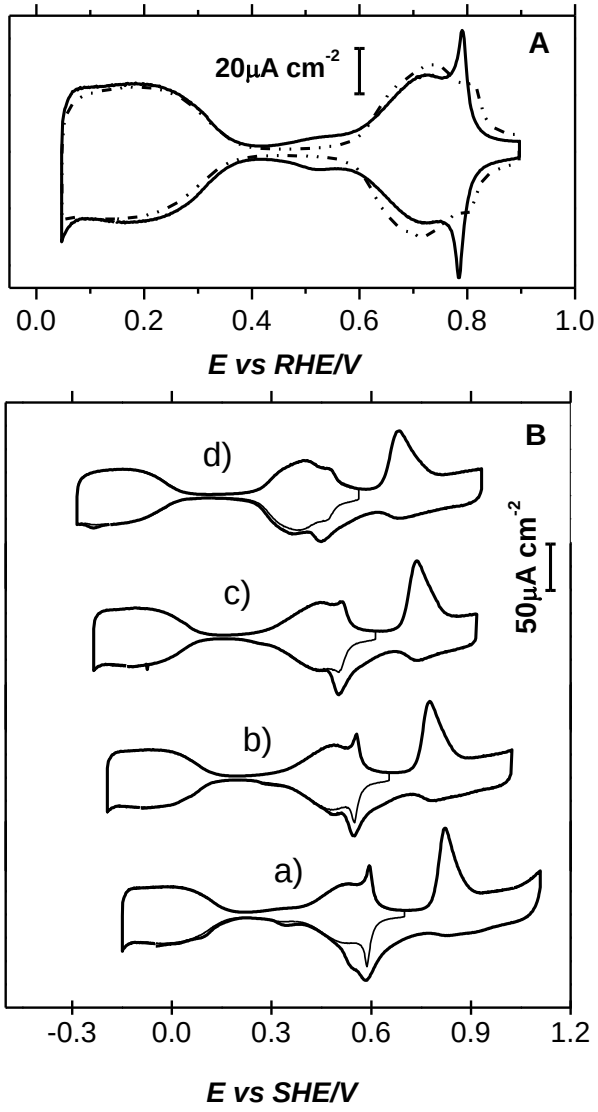

Figure 1: Cyclic voltammogram of Pt(111) in (0.1-x)M NaF + xM $HClO_4$ mixtures of different pH. A) At pH ca. 3.20 (solid line) and 5.70 (dashed line) in the RHE scale. Scan rate: 50mV/s B) At pH ca.: a) 3.20 (x=0.03), b) 4.15 (x=0.01), c) 4.85 (x=0.001), d) 5,70(x=0.0001) in the SHE scale. Scan rate: 50mV/s

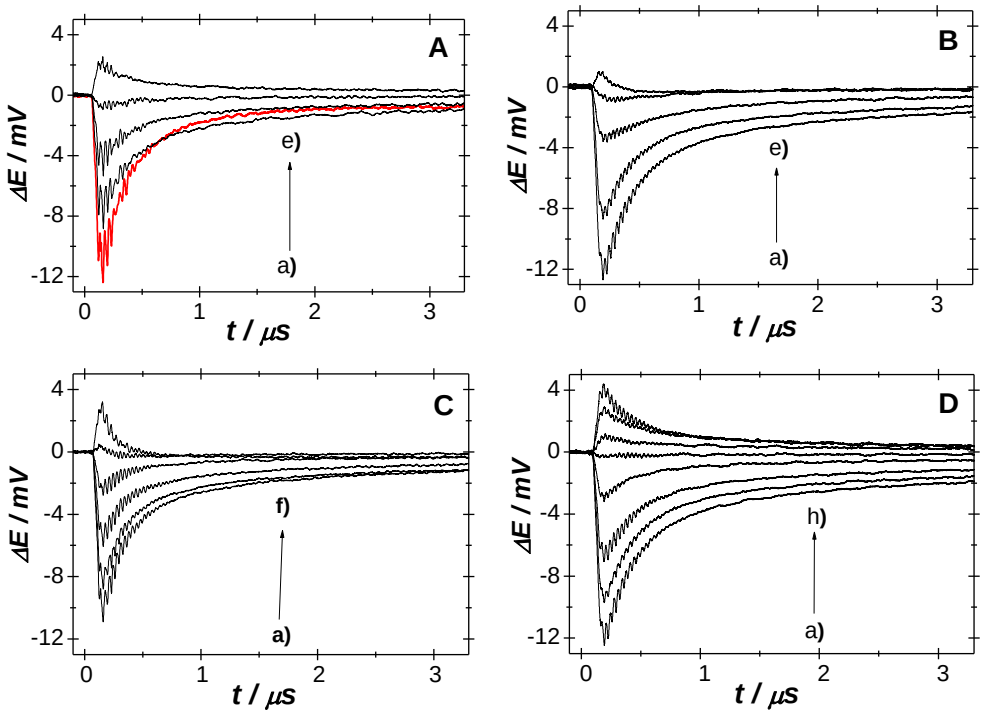

Figure 2: Laser-induced potential transients for Pt(111) in (0.1-x)M NaF + xM $HClO_4$ at mainly low applied potentials:

A) pH=3.2 (3): a) 150mV, b) 400mV, c) 450mV, d) 500mV, e) 550mV,

B) pH= 4.2 (4): a)150mV, b) .450mV, c) 530mV d) 570mV and e) 600mV,

C) pH=4.7 (5): a) 150mV, b) 450mV, c) 500mV, d) 550mV, e) 600mV and f) 700mV

D) pH=5.70 (6): a) 150mV, b) 500mV, c) 550mV, d) 600mV, e) 640mV, f) 650mV, g) 700mV and h) 750mV.

Energy beam: 1.5-1.8mJ. All given potentials are referenced to the RHE scale

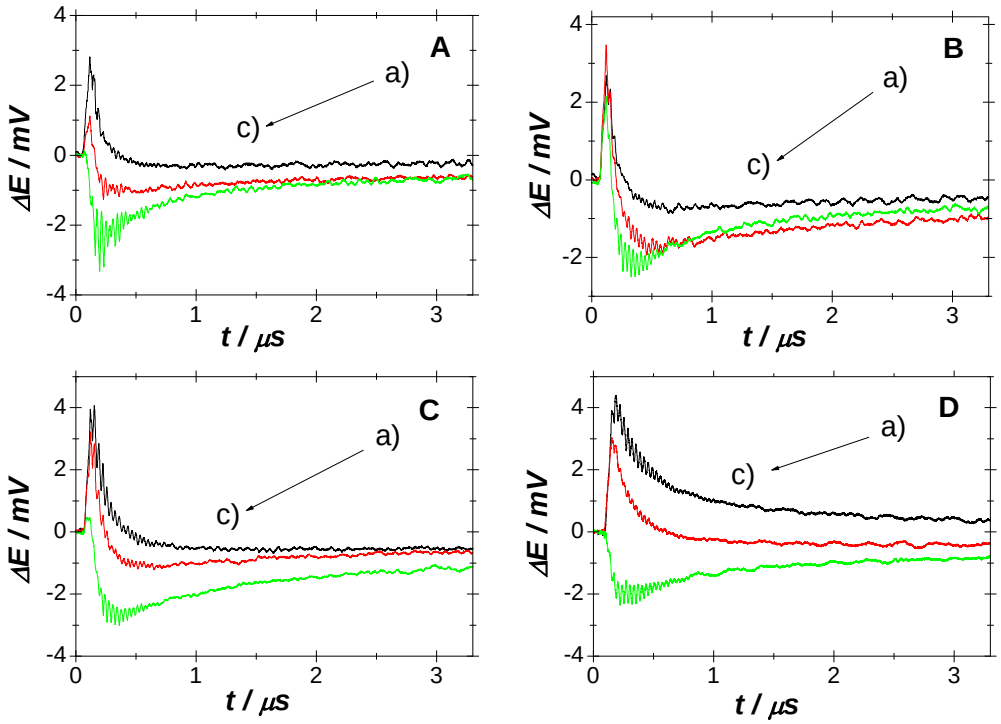

Figure 3: Laser-induced potential transients for Pt(111) in (0.1-x) M NaF + xM $HClO_4$ at positive applied potentials.

*A) pH=3.20 (3): a)650m V, b) **750**mV and c) 900mV,*

*B) pH= 4.20 (4): a)700V, b)**750**V and c) 800V*

*C) pH=4.7 (5): a)**750**mV, b) 900mV, c) 950mV*

*and D) pH=5.7 (6), a) **750**mV, b) 900mV, c) 950mV*

Energy beam: 1.5-1.8mJ. All given potentials are referenced to the RHE scale

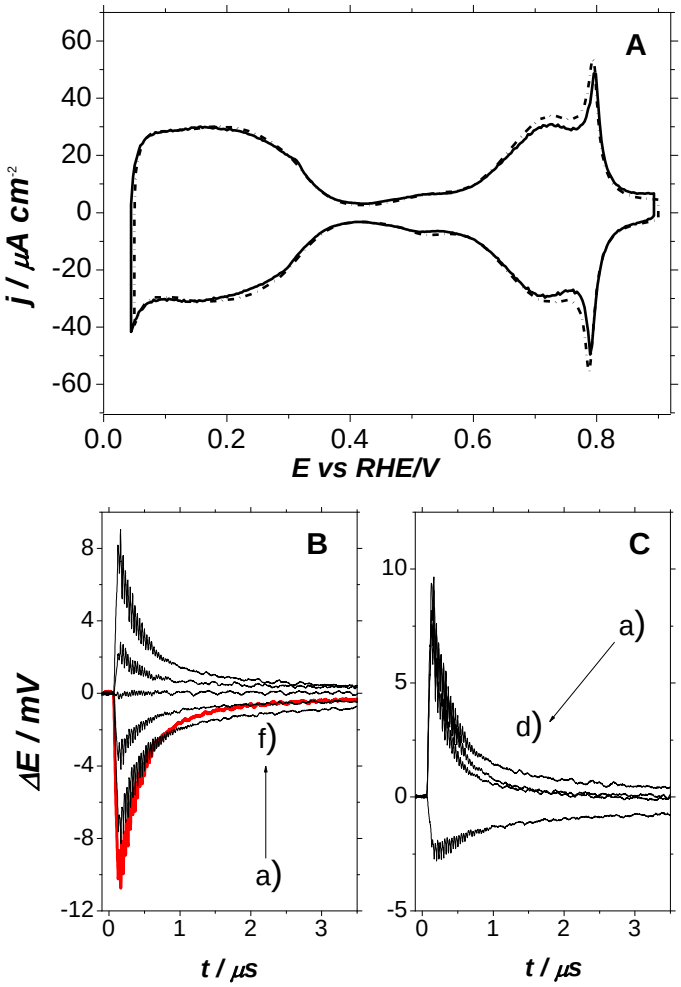

Figure 4: A) Cyclic voltammograms of Pt(111) in 0.1M $KClO_4$ + 1mM $HClO_4$ (solid line) and (0.1-x) M NaF + xM $HClO_4$, (dashed line), x= 0.03, pH≈3.20

Laser-induced potential transients (vs SHE) for Pt(111) in 0.1M $KClO_4$+ 1mM $HClO_4$.

B) a)150mV, b) 400mV, c) 450mV, d) 500mV, e) 550mV and f) 600mV

C) a)700mV, b) .800mV, c) 900mV and d) 1000mV

Energy beam: 1.70mJ. All given potentials are in the RHE scale.

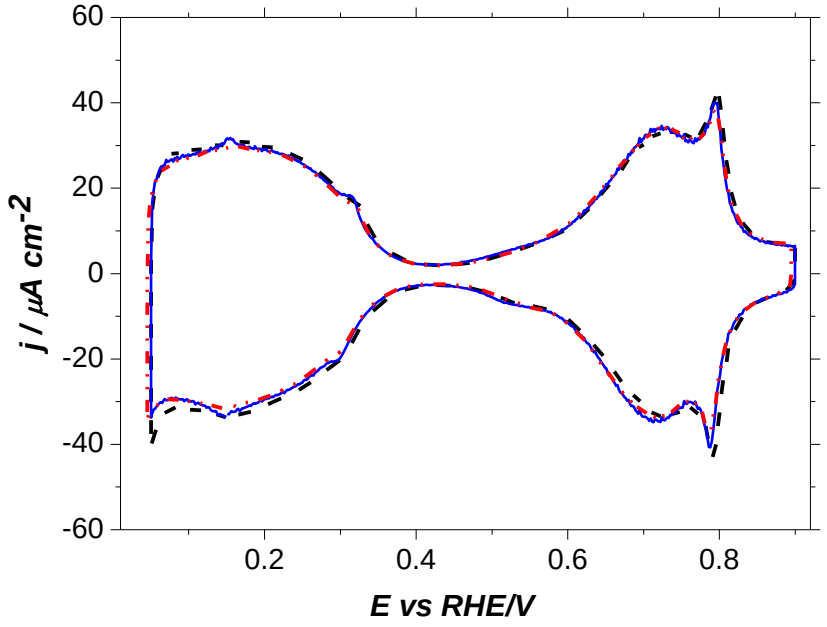

Figure 5: Cyclic voltammogram of Pt(111) in (0.1-x)M $KClO_4$ + xM NaF/$HClO_4$ buffer, pH=4, at three different buffer concentrations: dashed line) 0.05M, solid line) 0.02M and dotted line) 0.01M

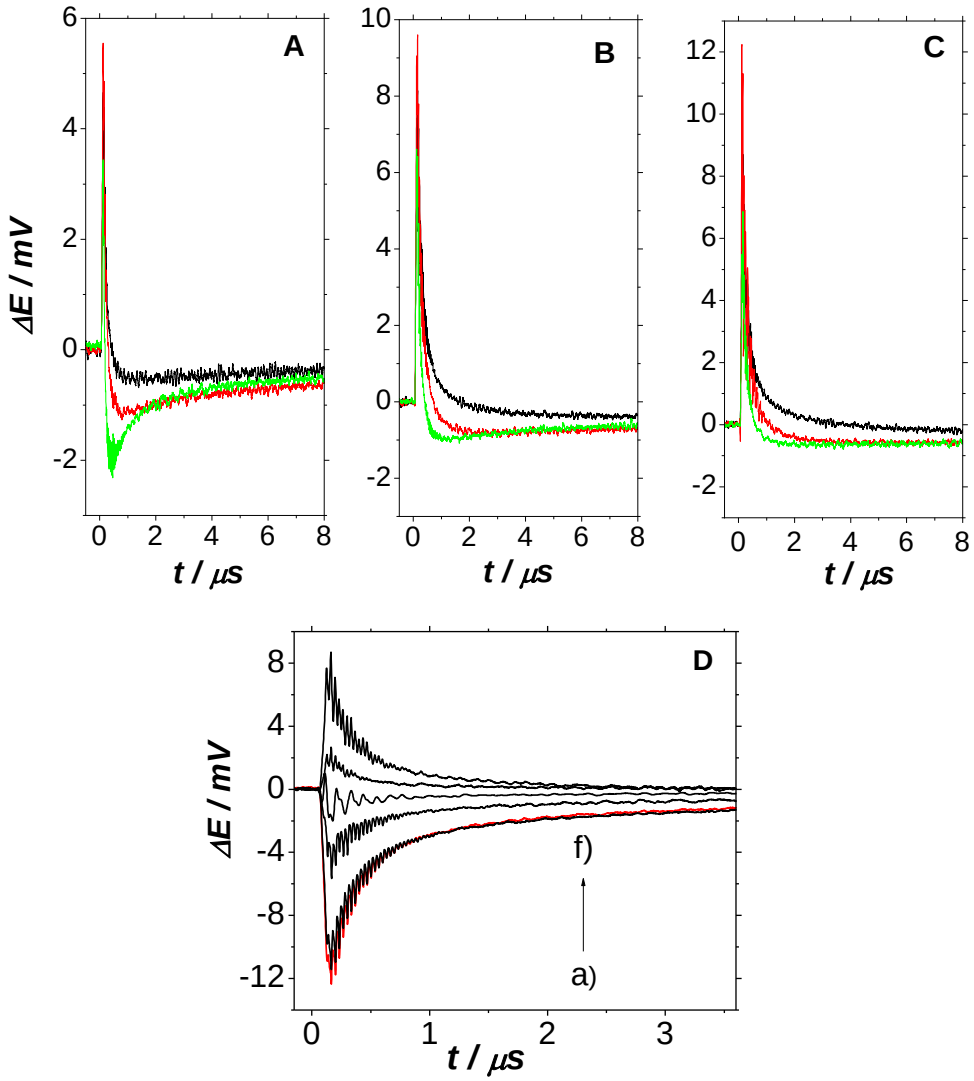

Figure 6:Potential laser transients at the applied potentials: 700mV, 800mV and 900mV, respectively, for the solutions (0.1-x)M $KClO_4$ + xM NaF/$HClO_4$ buffer, pH4, at three different buffer concentrations.

A) 0.05M $KClO_4$ + 0.05M NaF+0.005M $HClO_4$

B) 0.08M $KClO_4$ + 0.02M NaF+0.002M $HClO_4$

C) 0.09M $KClO_4$ + 0.01M NaF+0.001M $HClO_4$

D) Potential laser transients for the buffer solution: 0.09M $KClO_4$ +0.01M NaF/ $HClO_4$ buffer at different applied potentials: a) 150mV, b)400mV, c) 500mV, d) 550mV, e) 600mV, f) 700mV.

Energy beam: 1.8mJ. All given potentials are referenced to RHE scale.

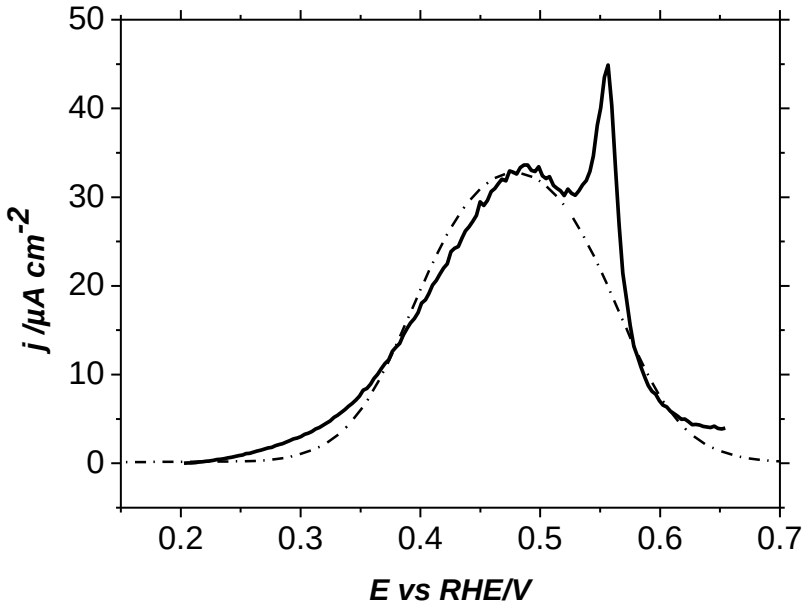

Figure 7: Comparison between experimental (solid line) voltammogram recorded at pH=4 and that simulated (dashed line) using a Frumkin isotherm with the parameters indicated in Table 1. Scan rate: 50mV/s

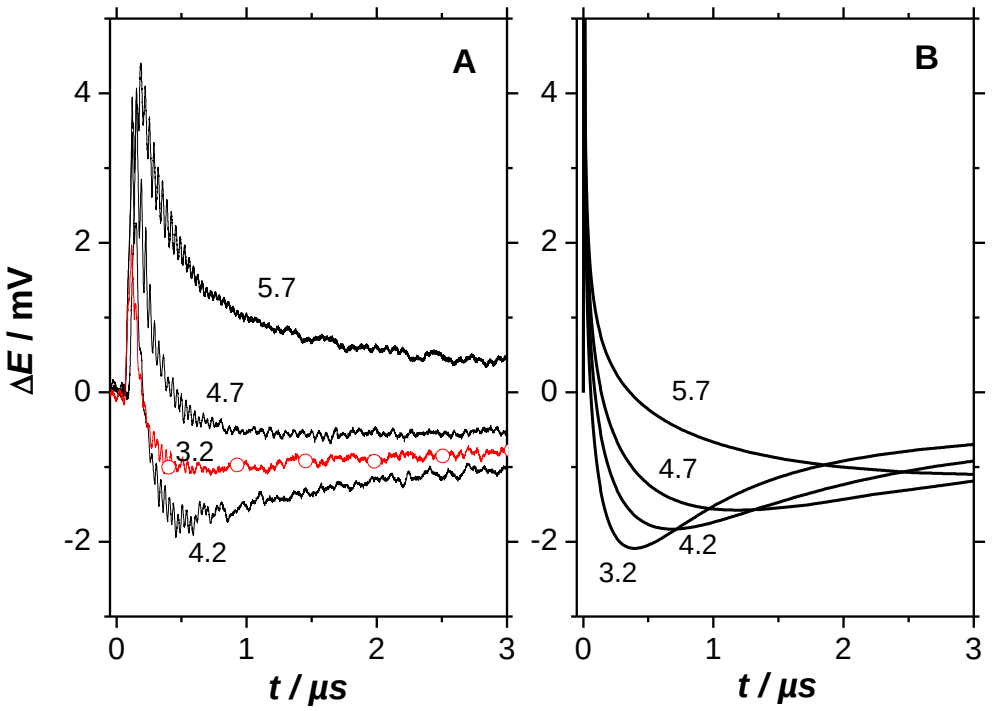

Figure 8: Comparison of experimental and simulated laser potential transients at different pH, as labelled in the figure, recorded at 0.75 V RHE. Laser intensity 1.7 mJ/pulse. In addition to the parameters indicated in table 1, the following parameters have been used for the simulation: $\left(\frac{\partial E}{\partial T}\right)_{q,\theta} = 0.21 mV\ K^{-1}$, log k_0/s^{-1}=6.25

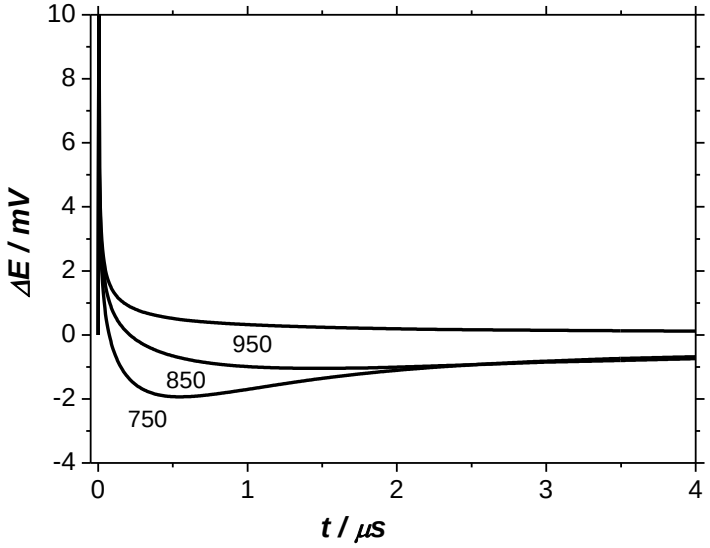

Figure 9: Simulated potential transients calculated with the same parameters as those used for figure 8 but varying the electrode potential, as labelled in the figure.

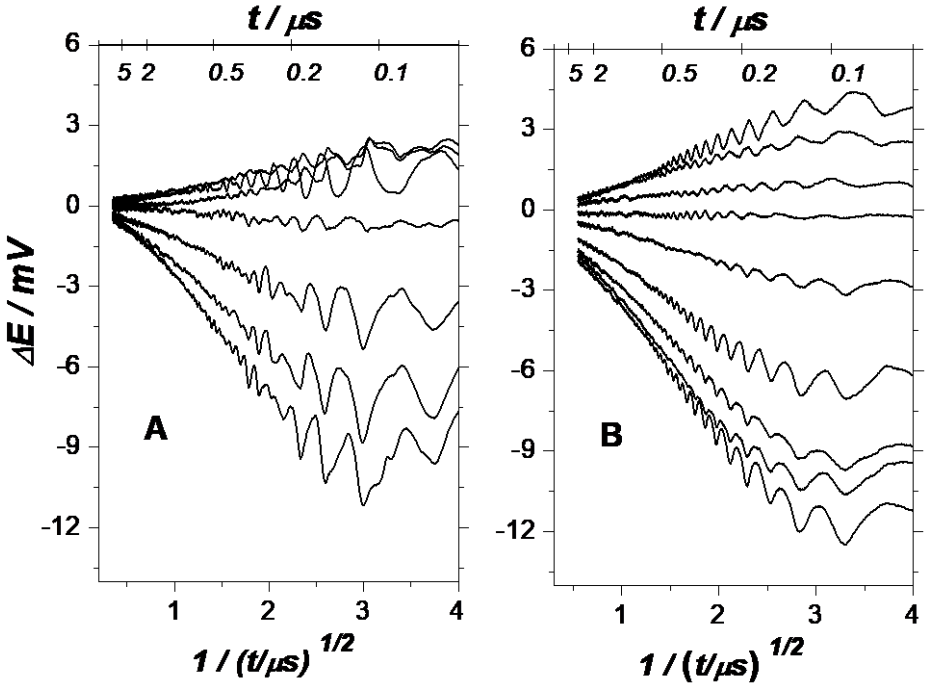

Figure10:

Change in the potential vs the inverse of the square root of the time for A) pH 3.35, from 400mV to 600mV vs SHE, B) pH 5.70 from 150V to 850mV vs RHE

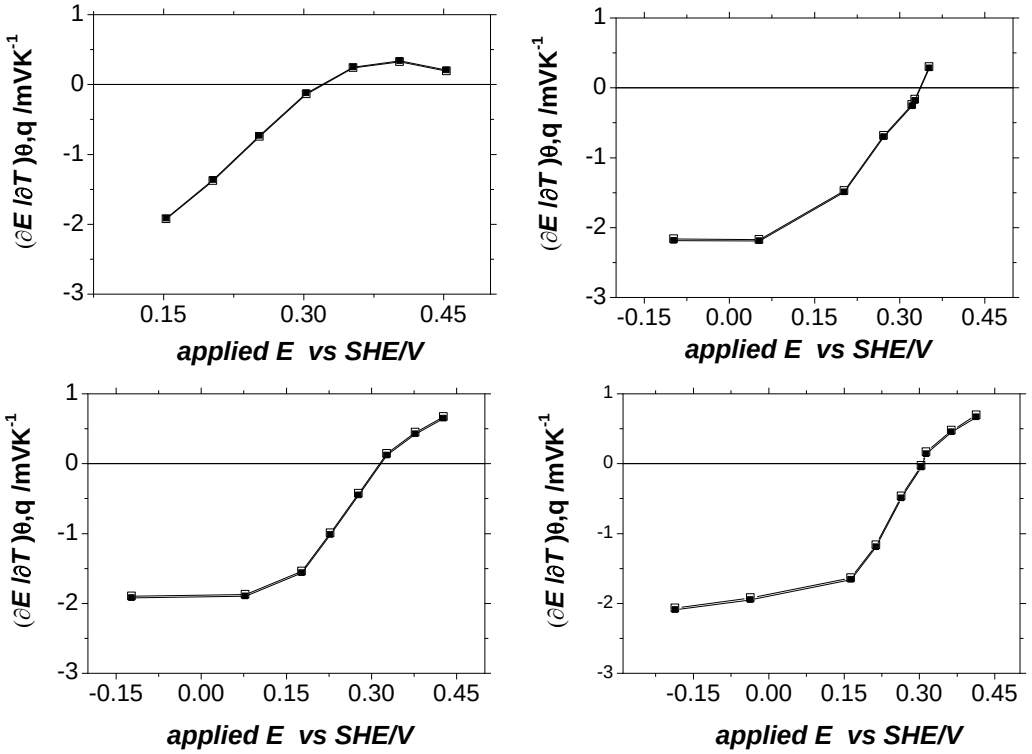

Figure 11:

Temperature coefficient of the double layer potential with (close symbols) and without (open symbols) the thermodifussion correction for Pt(111) in (0.1-x)M NaF + xM $HClO_4$: a) pH=3,20, b) pH=4,20, c)pH=4,65 and d) pH = 5.70.

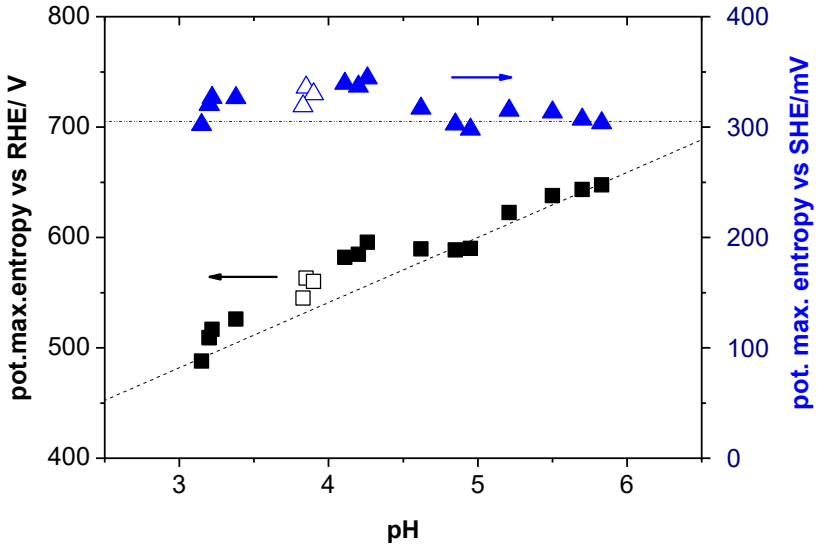

Figure 12: Plot of the pme values calculated at different pH at both RHE (squares) and SHE (triangles) scale. The dashed and dashed dotted lines corresponds to slopes of 59 and 0 mV/decade, respectively. assuming the pme is 305mV vs SHE. The closed symbols corresponds to buffer solutions of (0.1-x)M NaF + xM $HClO_4$ whereas open symbols are the pme calculated from the buffer solution 0.09M $KClO_4$ + 0.01M NaF/$HClO_4$.

pH	E^0/V	ω/kJ mol^{-1}	$q_{ML}/\mu Ccm^{-2}$	$\Delta S^0 / Jmol^{-1}K^{-1}$	$\frac{d\omega}{dT} / Jmol^{-1}K^{-1}$	*ref*
4	*0.675*	*7.84*	*120.5*	*-80[a]*	*-124[a]*	*this work*
1	*0.683*	*13.3*	*110*	*-96.7*	*-117*	*[47]*

Table 1: parameters resulting from the fit of a Frumkin isotherm to the cyclic voltammetry data. [a]values estimated from the fit of laser induced potential transients.

Ion	*S / J mol^{-1} K^{-1}*
OH^-	*53.90*
Na^+	*7.14*
ClO_4^-	*-3.10*
F^-	*11.50*
H^+	*39.39*
K+	*4.4*

Table 2: Ionic Entropies of Transport of Selected Ions from Ref[33]

(0.1-x) M NaF + xM $HClO_4$	
Ph	**[$\Delta E_{Thermodifusion}$ / ΔT] / mVK^{-1}**
3	*-0.031*
4	*0.018*
5	*0.026*
6	*0.027*
(0.1-x)M $KClO_4$ + xM $NaF/HClO_4$ buffer (pH=4)	
Solution	**[$\Delta E_{Thermodifusion}$ / ΔT] / mVK^{-1}**
0.05M $KClO_4$ + 0.05M $NaF/HClO_4$	*-0.016*
0.08M $KClO_4$ + 0.02M $NaF/HClO_4$	*-0.031*
0.09M $KClO_4$ + 0.01M $NaF/HClO_4$	*-0.036*

Table 3 : Contribution of the thermodiffusion potentials to the overall thermal coefficient of the potential drop for the different solutions employed in this work, calculated using the transport numbers obtained from the ionic mobilities at infinite dilution[50]

REFERENCES*:*

[1] H. Ogasawara, B. Brena, D. Nordlund, M. Nyberg, A. Pelmenschikov, L.G.M. Pettersson, A. Nilsson, Physical Review Letters, 89 (2002) 276102.
[2] M. Ito, M. Nakamura, Faraday Discuss., 121 (2002) 71-84.
[3] P.J. Feibelman, Science, 295 (2002) 99-102.
[4] J. Jupille, P. Pareja, J. Fusy, Surface Science, 139 (1984) 505-540.
[5] R. Vacha, V. Buch, A. Milet, J.P. Devlin, P. Jungwirth, Phys. Chem. Chem. Phys., 9 (2007) 4736-4747.
[6] V. Buch, A. Milet, R. Vacha, P. Jungwirth, J.P. Devlin, Proc. Natl. Acad. Sci. U. S. A., 104 (2007) 7342-7347.
[7] V. Lazarescu, J. Clavilier, Electrochimica Acta, 44 (1998) 931-941.
[8] T. Pajkossy, D.M. Kolb, Electrochim. Acta, 46 (2001) 3063-3071.
[9] A.N. Frumkin, O.A. Petrii, Electrochimica Acta, 20 (1975) 347-359.
[10] N. Garcia-Araez, V. Climent, E. Herrero, J.M. Feliu, J. Lipkowski, Electrochimica Acta, 51 (2006) 3787-3793.
[11] R.G. V.Climent, J.M. Orts, A. Aldaz and J.M. Feliu, in: B.E.C. C. Korzeniewski (Ed.) Electrochemical Society Proceedings, NY, 997, pp. 222.
[12] R.G. V. Climent, , J. M. Orts and J. M. Feliu, potential of zero total charge of pt single crystal electrodes, in: J.F.-M. Gregory Jerkiewicz, Branko N. Popov (Ed.) Hydrogen at Surface and Interfaces: Proceedings of the International Symposium, The Electrochemical Society, 2000, pp. 268.
[13] M.J. Weaver, Langmuir, 14 (1998) 3932-3936.
[14] A. Cuesta, Surface Science, 572 (2004) 11-22.
[15] R. Rizo, E. Sitta, E. Herrero, V. Climent, J.M. Feliu, Electrochimica Acta, 162 (2015) 138-145.
[16] R. Martínez-Hincapié, P. Sebastián-Pascual, V. Climent, J.M. Feliu, Electrochemistry Communications, 58 (2015) 62-64.
[17] A.N. Frumkin, O.A. Petrii, Electrochim. Acta, 20 (1975) 347-359.
[18] A.N. Frumkin, O.A. Petrii, B.B. Damaskin, Potential of Zero Charge, in: J.O.M. Bockris, B.E. Conway, E. Yeager (Eds.) Comprehensive Treatise of Electrochemistry, vol. 1. Plenum, New York, 1980, pp. 221-289.
[19] J.F. Smalley, C.V. Krishnan, M. Goldman, S.W. Feldberg, I. Ruzic, Journal of Electroanalytical Chemistry and Interfacial Electrochemistry, 248 (1988) 255-282.
[20] V.A. Benderskii, G.I. Velichko, Journal of Electroanalytical Chemistry and Interfacial Electrochemistry, 140 (1982) 1-22.
[21] V. Climent, B.A. Coles, R.G. Compton, Journal of Physical Chemistry B, 106 (2002) 5988-5996.
[22] V. Climent, B.A. Coles, R.G. Compton, Journal of Physical Chemistry B, 106 (2002) 5258-5265.
[23] S. Trasatti, Journal of Electroanalytical Chemistry and Interfacial Electrochemistry, 150 (1983) 1-15.
[24] S. Trasatti, Journal of Electroanalytical Chemistry and Interfacial Electrochemistry, 82 (1977) 391-402.
[25] N. Garcia-Araez, V. Climent, J.M. Feliu, J. Am. Chem. Soc., 130 (2008) 3824-3833.
[26] N. Garcia-Araez, V. Climent, J. Feliu, J. Phys. Chem. C, 113 (2009) 9290-9304.
[27] M. Osawa, M. Tsushima, H. Mogami, G. Samjeské, A. Yamakata, The Journal of Physical Chemistry C, 112 (2008) 4248-4256.
[28] V.C. Carol Korzeniewski, and Juan M. Feliu, Electrochemistry at Pt single Crystal Electrodes, Chapter Book, Electroanalytical Chemistry, in: Electroanalytical Chemistry. A Series of Advances, vol. 75, CRC Press, 2011.

[29] M. Kaack, D. Fick, Surf. Sci., 342 (1995) 111-118.
[30] O.A. Petrii, Russian Journal of Electrochemistry, 49 (2013) 401-422.
[31] G.N. Derry, J.Z. Zhang, Phys. Rev. B, 39 (1989) 1940-1941.
[32] H.H. Rotermund, S. Jakubith, S. Kubala, A. von-Oertzen, G. Ertl, J. Electron Spectrosc. Relat. Phenom., 52 (1990) 811-819.
[33] J.N. Agar, Advan. Electrochem. Electrochem. Eng., in: Wiley-Interscience (Ed.), vol. 2, New York, 1963, pp. 31.
[34] J.C. Huang, W.E. O'Grady, E. Yeager, Journal of the Electrochemical Society, 124 (1977) 1732-1737.
[35] F.T. Wagner, T.E. Moylan, Surface Science, 182 (1987) 125-149.
[36] F.T. Wagner, P.N. Ross, Journal of Electroanalytical Chemistry and Interfacial Electrochemistry, 250 (1988) 301-320.
[37] F.C. Nart, T. Iwasita, M. Weber, Electrochimica Acta, 39 (1994) 961-968.
[38] A. Lachenwitzer, N. Li, J. Lipkowski, J. Electroanal. Chem., 532 (2002) 85-98.
[39] Y. Cai, A.B. Anderson, The Journal of Physical Chemistry B, 109 (2005) 7557-7563.
[40] M. Zhao, A.B. Anderson, The Journal of Physical Chemistry Letters, 7 (2016) 711-714.
[41] H. Tanaka, S. Sugawara, K. Shinohara, T. Ueno, S. Suzuki, N. Hoshi, M. Nakamura, Electrocatalysis, 6 (2015) 295-299.
[42] M. Wakisaka, Y. Udagawa, H. Suzuki, H. Uchida, M. Watanabe, Energy Environ. Sci., 4 (2011) 1662-1666.
[43] A. Berná, V. Climent, J.M. Feliu, Electrochemistry Communications, 9 (2007) 2789-2794.
[44] Y. Marcus, Chemical Reviews, 109 (2009) 1346-1370.
[45] B. Hribar, N.T. Southall, V. Vlachy, K.A. Dill, Journal of the American Chemical Society, 124 (2002) 12302-12311.
[46] A.P. Sandoval, M.F. Suarez-Herrera, V. Climent, J.M. Feliu, Electrochem. Commun., 50 (2015) 47-50.
[47] V. Climent, R. Gómez, J.M. Orts, J.M. Feliu, J. Phys. Chem. B, 110 (2006) 11344-11351.
[48] J.M. Delgado, A. Berna, J.M. Orts, A. Rodes, J.M. Feliu, J. Phys. Chem. C, 111 (2007) 9943-9952.
[49] A. Berna, A. Rodes, J.M. Feliu, In-situ FTIR studies on the acid-base equilibria of adsorbed species on well-defined metal electrode surfaces, in: S.-G. Sun, P.A. Christensen, A. Wieckowski (Eds.) In-situ Spectroscopic Studies of Adsorption at the Electrode and Electrocatalysis, Elsevier, Amsterdam, 2007, pp. 1-32.
[50] C.R. Lide, CRC Handbook of Chemistry and Physics, 79 ed., CRC Press, Boca Raton, 1998.

TOC Figure